Computation of electron-impact rotationally elastic total cross sections for methanol over an extensive range of impact energy (0.1 – 2000 eV)

Journal Item

Computation of electron-impact rotationally elastic total cross sections for methanol over an extensive range of impact energy (0.1 – 2000 eV)

Minaxi Vinodkumar,[1,*] Chetan Limbachiya,[2] Avani Barot,[1] and Nigel Mason[3]
[1]*V.P. & R.P.T.P. Science College, Vallabh Vidyanagar-388 120, Gujarat, India*
[2]*P.S. Science College, Kadi-382 715, Gujarat, India*
[3]*Department of Physics & Astronomy, Open University, Milton Keynes, MK7 6AA, United Kingdom*
(Received 26 October 2012; published 4 January 2013)

Theoretical rotationally elastic total cross sections for electron scattering from methanol over the incident energy range 0.1–2000 eV are presented. The computation of such cross sections for methanol is reported over such an extended energy range. We have employed two distinct formalisms to compute the cross sections across this energy range; between 0.1 eV and the ionization threshold of the target we have used the *ab initio R*-matrix method, while at higher energies the spherical complex optical potential method is invoked. The results from both formalisms match quite well at energies where they overlap and hence imply that they are consistent with each other. These total cross-section results are also in very good agreement with available experimental data and earlier theoretical data. The composite methodology employed here is well established and can be used to predict cross sections for other targets where data is scarce or not available.

DOI: 10.1103/PhysRevA.87.012702 PACS number(s): 34.80.Bm

I. INTRODUCTION

Methanol or methylalcohol (CH_3OH) is the simplest volatile alcohol. Methanol is produced naturally as a part of the anaerobic metabolism of many varieties of bacteria, and is therefore ubiquitous in the environment, leading to a small fraction of methanol vapor being present in the terrestrial atmosphere. The main industrial applications of methanol are in the production of formaldehyde, acetic acid, and more recently in the formation of methyl esters used in the production of biodiesel. Studies on electron impact with methanol have gained prominence in recent years since electron interactions with methanol are important to the understanding of energy and material balances in combustion plasmas and also in the chemistry of such species in a terrestrial atmosphere. Moreover, such collision data play a pivotal role in modeling spark ignition in alcohol-fueled internal combustion engines [1,2]. The interest in electron-impact studies has also grown due to the discovery of the presence of methanol in interstellar space and in the atmospheres of planets in the solar system supporting ionospheres. In addition, methanol is an intermediate-sized molecule that can serve as a benchmark for developing theoretical models of electron interactions with larger biomolecules [3].

Theoretical models can be compared with experimental investigations. Recent studies of electron interactions with methanol include the experimental studies of Lee *et al.* [4] and Sugohara *et al.* [5], who measured the elastic cross sections (ECSs) using a relative flow technique and reported cross sections in the range of 100–1000 eV. Silva *et al.* [6] reported a total cross section (TCS) using the linear transmission method in the range of 60–500 eV while Khakoo *et al.* [7] reported ECSs using a relative flow method for impact energies 1–100 eV. Szmytkowski and Krzysztofowicz [8] used the linear transmission method and measured TCSs in the range of 0.8–250 eV, and Sueoka *et al.* [9] and Schmieder [10] measured TCSs in the range of 1–300 and 1.5–50 eV, respectively.

Previous theoretical studies include those of Bouchiha *et al.* [3], who calculated total elastic cross sections using the *ab initio R*-matrix formalism in the range of 0–15 eV. Khakoo *et al.* [7] calculated ECSs using the Schwinger multichannel method in the range 1–100 eV. Ming and Hua [11] calculated TCSs using the additivity rule in the range of 10–1000 eV. In our earlier work [12] we presented TCSs using the spherical complex optical potential (SCOP) formalism for impact energies from threshold to 2000 eV.

This review of previous work suggests that the studies on e-CH_3OH are fragmentary and that there are more experimental investigations compared to theory, and all previous authors have reported ECS-TCS over limited ranges of energy. In contrast, in the present paper we report electron-impact TCSs for methanol over an extensive range of impact energies from around a very low energy of 0.1 eV to a high energy of 2000 eV. Inspecting the range of incident energy it is quite clear that a single theoretical formalism cannot be employed for the entire energy range, hence we have partitioned the work into two prime energy regimes. Below 15 eV, we carried out *ab initio* calculations with a fixed nuclei approximation employing the UK molecular *R*-matrix method through QUANTEMOL-N software [13] and above the threshold of the target we employ the well-established SCOP formalism [14–16]. The two formalisms give consistent results at the transition energy (∼11 eV), enabling us to provide cross sections over such a wide range that such data will serve as an important database. The formation of transient anions (through scattering resonances) which may decay to produce neutral and anionic fragments are common phenomena at low impact energies below 10 eV and are very important in the understanding of the local chemistry of the electron-target interaction upon electron impact. Accordingly we also explore the formation of such resonances in low-energy scattering.

*minaxivinod@yahoo.co.in

TABLE I. Target properties obtained for the CH_3OH molecule.

Properties of CH_3OH	Present	Theoretical results	Experimental results
Ground-state energy (hartree)	−115.05	−115.14 (Ref. [3]); −115.26 (Ref. [17]); −115.01 (Ref. [3])	
First excitation energy (eV)	8.55	6.76 (Ref. [3]); 8.53 (Ref. [12])	6.5 (Ref. [19])
Rotational constant (cm^{-1})	4.11		4.25 (Ref. [18])
Dipole moment (D)	2.28	1.97 (Ref. [3])	1.81 (Ref. [7]); 1.70 (Ref. [18])

II. THEORETICAL METHODOLOGY

The present calculations employ two distinct methodologies, namely, the R matrix and the SCOP, which are appropriate in two distinct regimes of impact energies, one below the ionization threshold of the target and the other above it. Before going into the details about these two methodologies we discuss the target model employed for the low-energy calculations.

A. Target model used for low-energy calculations

The accuracy of the scattering data depends on the accuracy of the target wave function, hence, it is imperative to have an appropriate target model. Methanol is composed of single bonds, C-H with a bond length of $2.06a_0$, O-H with $1.8a_0$, and C-O with $2.68a_0$.We employed a double zeta plus polarization (DZP) basis set for the target wave-function representation and a C_s group of order four. For the optimized geometry of the target, the occupied and virtual molecular orbitals are obtained using Hartree-Fock self-consistent field (HF-SCF) optimization and were used to set up the CH_3OH electronic target states. The ground-state Hartree-Fock electronic configuration is $1a'$, $2a'$, $3a'$, $4a'$, $5a'$, $1a''$, $6a'$, $7a'$, and $2a''$. To establish a balance between the amounts of correlation incorporated in the target wave function, out of 18 electrons, we froze four electrons in two molecular orbitals $(1a',2a')$. The rest of the 14 electrons were allowed to move freely in the active space of ten target occupied and virtual molecular orbitals ($3a'$, $4a'$, $5a'$, $6a'$, $7a'$, $8a'$, $9a'$, $10a'$, $1a''$, and $2a''$). A total of 19 electronically excited target states were represented by 2598 configuration state functions (CSFs) for the ground state and the number of channels included in the calculation is 230. A large number of CSFs ensures the correct determination of the position of the resonance peak in the low-energy regime.

The present calculation yields the ground-state energy of CH_3OH as −115.05 hartree, which is in excellent agreement with theoretical value of −115.14 hartree [3], −115.26 hartree [17], and −115.01 hartree [3]. The present computed rotational constant of CH_3OH is 4.11 cm^{-1}, which is in agreement with the experimental value of 4.25 cm^{-1} reported in the Computational Chemistry Comparison and Benchmark Database (CCCBDB) [18]. The first electronic excitation energy of CH_3OH is found to be 8.55 eV using the configuration interaction (CI) model, which agrees well with the calculated value of 8.53 eV reported by Vinodkumar *et al.* [12], albeit higher compared to the theoretical value of 6.76 eV reported by Bouchiha *et al.* [3] and the experimental value of 6.5 eV reported by Knoop *et al.* [19]. The present dipole moment is 2.28 D, which is slightly higher compared to the theoretical value of 1.97 D [3] and the measured values of 1.81 D [7] and 1.70 D [18]. The target properties along with available comparisons are listed in Table I. The 19 electronic excitation thresholds for methanol are listed in Table II.

B. Low-energy formalism (0.1 to ∼15 eV)

The most popular methodologies employed for low-energy electron collision calculations are the Kohn variational method [20,21], the Schwinger variational method [22–24], and the R-matrix method, of which the R matrix is the most widely used. The underlying idea behind the R-matrix method relies on the division of configuration space into two spatial regions, namely, the inner region and the outer region. This spatial distribution is a consequence of electronic charge distribution around the center of mass of the system. The inner region is so chosen that it accommodates the total wave function of the target plus the scattering electrons. Thus all of the N target electrons plus one scattering electron are contained in the inner region, which makes the problem numerically complex but very precise. The interaction potential consists of short-range potentials which are dominant in this region, e.g., static, exchange, and correlation polarization potentials. The solution of the inner region problem involves rigorous quantum chemistry methods and thus consumes the maximum time of the calculation. However, the inner region problem is solved independent of the energy of the scattering electron and hence is done only once. In the outer region when the scattering electron is at a large distance from the center of mass of the target, the probability of swapping its identity with any one of the target electrons is negligible, resulting in a negligible contribution from the exchange and correlation effects. The only long-range multipolar interactions between

TABLE II. Vertical excitation energies for all states of CH_3OH.

State	Energy (eV)	State	Energy (eV)	State	Energy (eV)	State	Energy (eV)
$1A'$	0.0	$1A'$	11.16	$3A''$	12.73	$1A''$	13.74
$3A''$	8.55	$3A'$	11.26	$3A''$	13.42	$3A'$	14.09
$1A'$	8.96	$1A''$	11.42	$1A''$	13.59	$1A'$	14.54
$3A'$	10.35	$1A'$	12.19	$1A'$	13.62	$3A'$	14.82
$3A''$	11.03	$3A'$	12.54	$3A'$	13.68		

the scattering electron and the target are included. A single center close-coupling approximation with direct potentials leads to a set of coupled differential equations here, and this provides quick, simple, and fast solutions in the outer region. For the present system the inner R-matrix radius is taken as $12a_0$.

The main task in the present scattering calculation lies in the solution of the time-independent Schrödinger equation. For this the inner region wave function is constructed using a close-coupling approximation [25]. For the inner region the total wave function for the system is expressed as

$$\psi_k^{N+1} = A \sum_I \psi_I^N (x_1, \ldots, x_N) \sum_j \zeta_j(x_{N+1}) a_{Ijk} + \sum_m \chi_m(x_1, \ldots, x_{N+1}) b_{mk}, \quad (1)$$

where A is the antisymmetrization operator that takes care of the exchange effect, x_N is the spatial and spin coordinate of the nth electron, ξ_j is a continuum orbital spin coupled with the scattering electron, and a_{Ijk} and b_{mk} are variational coefficients determined by the diagonalization of the $N+1$ Hamiltonian in the calculation. The accuracy of the calculation depends solely on the accurate construction of this wave function given in Eq. (1). The first summation runs over the target states used in the close-coupled expansion and a static-exchange calculation has a single Hartree-Fock target state in the first sum. The χ_m's are multicenter quadratically integrable functions, constructed from target occupied and virtual molecular orbitals, and are used to represent the correlation and polarization effects. This sum runs over the minimal number of configurations, usually three or fewer, which is required to relax the orthogonality constraints between the target molecular orbitals and the functions used to represent the configuration. The continuum orbitals are centered on the center of mass of the molecule. These orbitals do not vanish on the R-matrix boundary as they are of longer range than the molecular bound orbitals that are centered on the nuclei. Our fully close-coupled calculation uses the lowest number of target states, represented by a configuration interaction (CI) expansion in the first term and over 100 configurations in the second. These configurations allow for both orthogonality relaxation and short-range polarization effects.

The complete molecular orbital representation in terms of occupied and virtual target molecular orbitals is constructed using the Hartree-Fock self-consistent field method with Gaussian-type orbitals (GTOs) and the continuum orbitals of Faure *et al.* [26] and include up to g ($l = 4$) orbitals. The benefit of employing a partial-wave expansion for a low-energy electron molecule interaction is its rapid convergence. For polar molecules, due to the presence of a long-range dipole interaction, the elastic cross section is divergent in the fixed nuclei approximation at low impact energies. To obtain the converged results the effect of rotation must be included along with a very large number of partial waves. Thus in the case of dipole-forbidden excitations ($\Delta J \neq 1$), where J represents the rotational quantum number, the convergence of the partial waves is rapid, but in the case of dipole-allowed excitations ($\Delta J = 1$) the partial-wave expansion converges slowly due to the long-range nature of the dipole interaction. In order to account for the higher partial waves not included in the fixed nuclei T matrices, the closure formula that involves the Born correction is applied. The effect of partial waves higher than $l = 4$ was included using a Born correction which requires expressions for the partial waves as well as full Born cross sections. These expressions are used from the work of Chu and Dalgarno [27]. The low partial-wave contribution arising from the Born correction is therefore subtracted in order that the final rotational cross-section set contains only those partial waves due to the R-matrix calculation. We are constrained to employ partial waves for the continuum orbital up to $l = 4$ only, as the representation in Gaussian-type orbitals for Bessel functions higher than $l = 4$ is not available. For low partial waves ($l \leqslant 4$) the T matrices computed from the R-matrix calculations are employed to compute the cross sections. The low partial-wave contribution arising from the Born contribution is subtracted in order that the final cross-section set only contains those partial waves due to the R-matrix calculation. We have performed the calculations with and without the dipole Born correction.

The R matrix provides the link between the inner region and the outer region. The R matrix is propagated to an asymptotic region where the radial wave functions describing the scattering electron can be matched to analytical expressions. For this purpose the inner region is propagated to the outer region potential until its solutions match with the asymptotic functions given by the Gailitis expansion [28]. Coupled single center equations describing the scattering in the outer region are integrated to identify the K-matrix elements. The K matrix is a symmetric matrix whose dimensions are the number of open channels. All the observables can be deduced from it and further it can be used to obtain T matrices by using the definition

$$T = \frac{2iK}{1 - iK}. \quad (2)$$

The T matrices are in turn used to obtain various total cross sections. The K matrix is diagonalized to obtain the eigenphase sum. The eigenphase sum is further used to obtain the position and width of the resonance [27].

C. High-energy formalism

High-energy electron scattering is modeled using the well-established SCOP formalism [29,30], which employs a partial-wave analysis to solve the Schrödinger equation with various model potentials as its input. The interaction of the incoming electron with the target molecule can be represented by a complex potential comprising real (V_R) and imaginary parts (V_I) as

$$V_{\text{opt}}(E_i, r) = V_R(E_i, r) + i V_I(E_i, r), \quad (3)$$

such that

$$V_R(r, E_i) = V_{\text{st}}(r) + V_{\text{ex}}(r, E_i) + V_p(r, E_i), \quad (4)$$

where the real part V_R comprises the static potential (V_{st}), exchange potential (V_{ex}), and polarization potential (V_p). The static potential (V_{st}) is calculated at the Hartree-Fock level. The exchange potential (V_{ex}) term accounts for the electron exchange interaction between the incoming projectile and one of the target electron. The polarization potential (V_p) represents approximately the short-range correlation and long-range

polarization effect arising from the temporary redistribution of the target charge cloud. Note that the spherical complex optical potential (SCOP) as such does not require any fitting parameters. The most important basic input for evaluating all these potentials is the charge density of the target. We have used the atomic charge density derived from the Hartree-Fock wave functions of Bunge *et al.* [31]. The *e*-molecule system is more complex as compared to the *e*-atom system. The complexity is reduced by adopting a single center approach [32] so as to make the spherical approximation applicable. In the case of CH_3OH we employ the group additivity rule [33] and identify two prime scattering centers (C and O) from the geometry of the target. The two groups are CH_3 and OH. In the case of CH_3 and OH, we reduce the system to single center by expanding the charge density of the lighter hydrogen atoms at the center of the heavier carbon or oxygen atom by employing the Bessel function expansion given in Gradshetyn and Ryzhik [34]. The spherically averaged molecular charge density $\rho(r)$ is determined from the constituent atomic charge density using the Hartree-Fock wave functions of Bunge *et al.* [31]. The molecular charge density $\rho(r)$ so obtained is renormalized to incorporate the covalent bonding [35]. In the SCOP method, the spherical part of the complex optical potential is treated exactly in a partial-wave analysis to yield various cross sections [15]. Here we have neglected the nonspherical terms arising from the vibrational and rotational excitation in the full expansion of the optical potential.

The atomic charge densities and static potentials ($V_{\rm st}$) are formulated from the parametrized Hartree-Fock wave functions given by Bunge *et al.* [31]. The parameter-free Hara's 'free-electron gas exchange model' [36] is used to generate the exchange potential ($V_{\rm ex}$). The polarization potential (V_p) is constructed from the parameter-free model of correlation-polarization potential given by Zhang *et al.* [37]. Here, various multipole nonadiabatic corrections are incorporated into the intermediate region which will smoothly approach the correct asymptotic form at large r. In the low-energy region, the small r region is not important due to the fact that higher-order partial waves are unable to penetrate the scattering region. However, in the present energy region, a large number of partial waves contribute to the scattering parameters and correct short-range behavior of the potential is essential.

The imaginary part in $V_{\rm opt}$ is called the absorption potential, $V_{\rm abs}$ or V_I, and accounts for the total loss of flux scattered into the allowed electronic excitation or ionization channels. The $V_{\rm abs}$ is not a long-range effect and its penetration towards the origin increases with an increase in the energy. This implies that at high energies the absorption potential accounts for the inner-shell excitations or ionization processes that may be closed at low energies.

The well-known quasi-free-model form of Staszeweska *et al.* [38,39] is employed for the absorption part given by

$$V_{\rm abs}(r,E_i) = -\rho(r)\sqrt{\frac{T_{\rm loc}}{2}}\left(\frac{8\pi}{10k_F^3E_i}\right)\theta\left(p^2-k_F^2-2\Delta\right) \times (A_1+A_2+A_3), \tag{5}$$

where the local kinetic energy of the incident electron is

$$T_{\rm loc} = E_i - (V_{\rm st}+V_{\rm ex}+V_p), \tag{6}$$

and where $p^2 = 2E_i$, $k_F = [3\pi^2\rho(r)]^{1/3}$ is the Fermi wave vector, and A_1, A_2, and A_3 are dynamic functions that depend differently on $\theta(x)$, I, Δ, and E_i. Here, I is the ionization threshold of the target, $\theta(x)$ is the Heaviside unit step function, and Δ is an energy parameter below which $V_{\rm abs} = 0$. Hence, Δ is the principal factor which decides the values of the total inelastic cross section, since below this value ionization or excitation is not permissible. This is one of the main characteristics of the Staszewska model [38,39]. In the original Staszewska model [38,39] $\Delta = I$ is considered and hence it ignores the contributions coming from discrete excitations at lower incident energies. This has been realized earlier by Garcia and Blanco [40,41] who elaborately discussed the need to modify Δ value. This has been attempted by us by considering Δ as a slowly varying function of E_i around I. Such an approximation is meaningful since Δ fixed at I would not allow excitation at the energies $E_i \leqslant I$. However, if the Δ is much less than the ionization threshold, then $V_{\rm abs}$ becomes unexpectedly high near the peak position. The amendment introduced by us is to give a reasonable minimum value of $0.8I$ to Δ [42] and also to express the parameter as a function of E_i around I, i.e.,

$$\Delta(E_i) = 0.8I + \beta(E_i - 1). \tag{7}$$

Here the value of the parameter β is obtained by requiring that $\Delta = I$ (eV) at $E_i = E_p$, the value of incident energy at which $Q_{\rm inel}$ reaches its peak. E_p can be found by calculating $Q_{\rm inel}$ by keeping $\Delta = I$. Beyond E_p, Δ is kept constant and is equal to the ionization threshold I. The theoretical basis for assuming a variable Δ is discussed in more detail by Vinodkumar *et al.* [33]. Expression (7) is meaningful since if Δ is fixed at the ionization potential it would not allow any inelastic channel to open below I, and also, if it is very much less than I, then $V_{\rm abs}$ become significantly high close to the peak position of $Q_{\rm inel}$.

The complex potential thus formulated is used to solve the Schrödinger equation numerically through partial-wave analysis. This calculation will produce complex phase shifts for each partial wave which carries the signature of interaction of the incoming projectile with the target. At low impact energies only a few partial waves are significant, but as the incident energy increases more partial waves are needed for convergence. The phase shifts (δ_l) thus obtained are employed to find the relevant cross sections, and total elastic ($Q_{\rm el}$) and the total inelastic cross sections ($Q_{\rm inel}$) using the scattering matrix $S_l(k) = \exp(2i\delta_l)$ [42]. The total cross sections such as the total elastic ($Q_{\rm el}$) and the total inelastic cross sections ($Q_{\rm inel}$) can be derived from the scattering matrix [29]. The sum of these cross sections will then give the total scattering cross section (TCS) Q_T [30].

III. RESULTS AND DISCUSSION

In the present paper, we have performed a comprehensive computation of the total cross sections for electrons colliding with methanol in the gas phase. The main goals of the present work are twofold: to detect the resonance structure at low energies that may lead to fragmentation of the molecule (which is performed by studying the eigenphase diagram) and to provide total scattering cross sections over a wide range of impact energies from 0.1 to 2000 eV. The calculations were

TABLE III. Total electron scattering cross sections for CH_3OH in ($Å^2$).

	TCS			
Energy (eV)	Without Born correction	With Born correction	Energy (eV)	TCS
0.1	49.51	1290.27	11	24.99
0.5	32.42	363.58	13	24.89
0.6	31.09	315.22	15	24.37
0.7	30.07	279.53	17	23.74
0.8	29.25	252.03	20	22.77
0.9	28.54	230.11	25	21.26
1.0	27.89	212.17	30	19.86
1.3	26.20	173.48	35	18.57
1.5	25.22	155.49	40	17.40
2.0	23.32	124.95	45	16.36
2.5	22.16	105.81	50	15.44
3.0	21.52	92.75	60	13.95
3.5	21.19	83.28	70	12.80
4.0	21.02	76.09	80	11.87
4.5	20.99	70.45	90	11.10
5.0	21.09	65.97	100	10.45
5.5	21.34	62.39	150	8.27
6.0	21.75	59.54	200	6.95
6.5	22.29	57.29	250	6.03
7.0	22.92	55.53	300	5.34
7.5	23.59	54.15	500	3.69
8.0	24.21	53.03	800	2.55
8.5	24.65	52.02	900	2.32
9.0	24.86	51.02	1000	2.13
9.5	24.84	49.91	1500	1.52
10.0	24.86	48.74	2000	1.18

carried out using the fixed nuclei static-exchange-polarization approximation at the equilibrium geometry of the ground state of CH_3OH. The theoretical formalisms have their own limitations over the range of impact energies. More elaborately, the *ab initio* calculations are computationally viable only up to around 20 eV, while the SCOP formalism could be employed successfully from threshold of the target to 2000 eV. In the present work we computed the total cross section below the ionization threshold using a close-coupling formalism employing the *R*-matrix method and beyond the ionization threshold we used the SCOP formalism. The results obtained from the two different methods are consistent and there is a smooth transition at the overlap of the two formalisms. Thus, it is possible to provide the total cross section over a wide range of impact energies from meV to keV for a variety of targets [43–47]. We have presented our results in graphical form (Figs. 1–6) and the numerical values are tabulated in Table III.

For methanol, three core excited resonances have been detected experimentally below the threshold of the first excited state. A resonance with $2A''$ symmetries was located at 6.4 eV by Skalicky and Allan [48], at 6.5 eV by Prabhudesai *et al.* [49], and calculated by Bouchiha *et al.* [3] to lie at 6.75 eV. A second resonance with $2A'$ symmetries was identified at 7.9 eV by Skalicky and Allan [48], 8 eV by Prabhudesai *et al.* [49], and calculated by Bouchiha *et al.* [3] to be at 8.81 eV, and a third

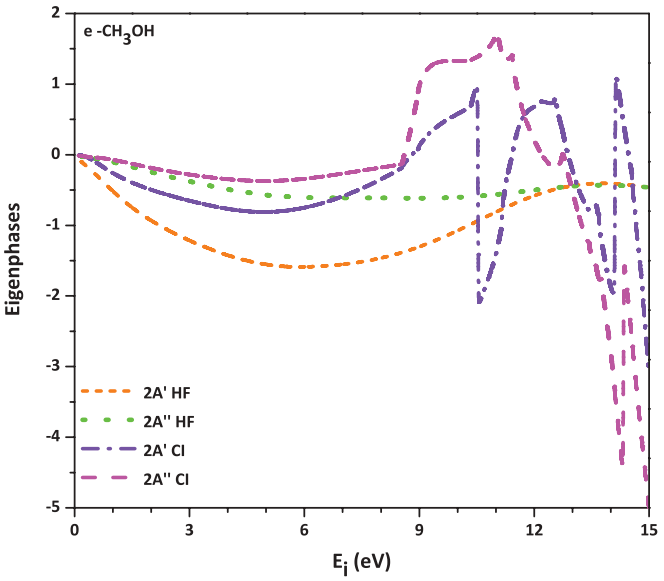

FIG. 1. (Color online) Eigenphase sums of e-CH_3OH for a 19-state CC calculation.

resonance with $2A'$ symmetry was found around 10.5 eV by Skalicky and Allan [48], 10.2 eV by Prabhudesai *et al.* [49], and calculated by Bouchiha *et al.* [3] to be at 11.73 eV [3]. Figure 1 shows the eigenphase diagram for two doublet scattering states ($2A'$ and $2A''$) of the CH_3OH system using HF and CI models. It is very clear from the figure that the inclusion of the polarization effect increases the eigenphase sum. The eigenphase diagrams reveal the position of the resonances in the low-energy regime. In the present calculation, the $2A''$ state shows a prominent structure at 8.5 eV, which is in agreement with the earlier predicted values of 8.81 eV [3], 7.9 eV [48], and 8.0 eV [49]. Similarly, another structure is seen in the $2A'$ state at 10.57 eV, which is in agreement with earlier reported values of 11.71 eV [3], 10.5 eV [48], and 10.2 eV [49], which can be visualized as a peak around 11 eV in the TCS curve. It is to be noted that as more states are included in the close-coupling (CC) expansion and retained in the outer region calculation, the eigenphase sum increases, reflecting the improved modeling of the polarization interaction.

The present calculated resonance positions (eV) are summarized in Table IV, where they are compared with earlier data. These resonances lead to the fragmentation of the molecule and the production of a variety of ions and radicals (H^-, O^-, OH^-, CH_3O^-, or CH_2OH^-). In the case of CH_3OH, the first two resonances produce only H^- and CH_3O^- whereas the third one

TABLE IV. The resonance positions (eV).

	Resonance position (eV)	
Symmetry	Present	Previous values
$2A''$	8.50	8.81 (Ref. [3])
		8.0 (Ref. [48])
		7.9 (Ref. [49])
$2A'$	10.57	11.73 (Ref. [3])
		10.5 (Ref. [48])
		10.2 (Ref. [49])

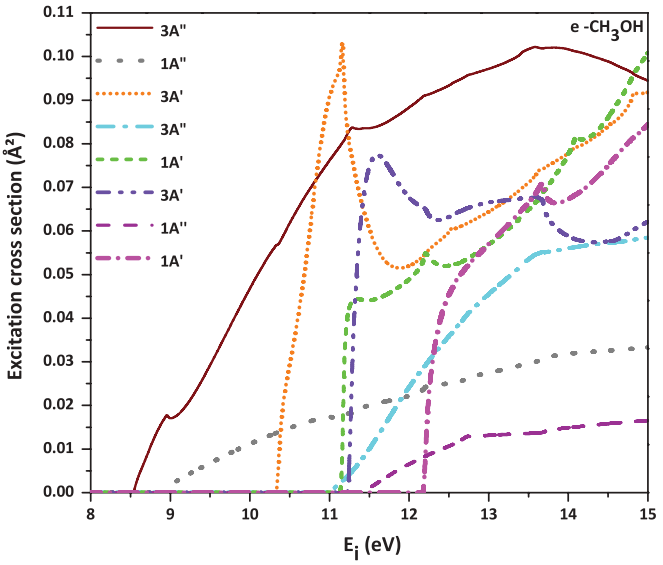

FIG. 2. (Color online) Electronic excitation cross sections of e-CH_3OH for a 19-state CC calculation from an initial state $1A'$.

also leads to the formation of O^-. It has also been observed that at the third resonance the hydrogen atom scrambles [50,51], revealing a larger lifetime against dissociation for this state. This is consistent with a Rydberg-like nature of the excited state seen in the absorption spectrum. It may be noted that even at this resonance the cross section for the formation of H^- is larger than that for the formation of O^-.

The total inelastic channel includes two important scattering processes, viz., ionization and electronic excitation. Below the ionization threshold of the target, the contributing channel to the total inelastic cross sections is predominantly electronic excitation. Figure 2 displays the electronic excitation cross sections from the ground state ($1A'$) to eight low-lying excited states ($3A''$, $1A''$, $3A'$, $3A''$, $1A'$, $3A'$, $1A''$, and $1A'$). It can be seen that the threshold of the first electronic excitation energy for CH_3OH is 8.5 eV. The electronic excitations to $3A'$ and $1A'$ show sharp increases near their respective thresholds which show the dominance of these energy levels in the present calculation. The notable structure in $3A'$ around 11 eV is reflected as a broad peak around 11 eV in TCSs and is in accordance with the experimental prediction of Skalicky and Allan [48] at 11.82 eV. Beyond 12 eV no prominent structures are observed.

The study of differential cross sections (DCSs) is very important as they are more accurately measured experimentally, and provides a stringent test for any scattering theory employed as it is sensitive to effects which are averaged out in the integral cross sections. Hence, we have calculated DCSs for the elastic scattering of electrons from CH_3OH at incident energies 5, 10, 15, and 20 eV in the angular range from 0° to 180°. Figures 3(a)–3(d) depict the behavior of DCSs as a function of angle theta (q) for incident energies 5, 10, 15, and 20 eV, respectively. We have compared the present DCS results with the experimental and theoretical results of Khakoo *et al.* [7] for the incident energies 5, 10, 15, and 20 eV while the theoretical results of Lee *et al.* [4] are reported for incident energies 5 and 10 eV. Khakoo *et al.* [7] have used the Schwinger multichannel pseudopotential method (SWCPP) and the Schwinger multichannel all electron method (SMCAE) to compute DCSs. For energies below 10 eV, the Static Exchange Polarization (SEP) model is considered and above it only the Static Exchange (SE) model is used by them [7]. So no absorption effects are considered in the calculation. Lee *et al.* [4] have used the complex scattering potential to compute the DCS. We have employed the close-coupling R-matrix method for the computation of DCSs. It can be noticed from Figs. 3(a)–3(d) that in general there is good accord of the present results with the experimental and theoretical results of Khakoo *et al.* [7] as well as the theoretical results of Lee *et al.* [4]. At 5 eV, the hump in the experimental results of Khakoo *et al.* [7] around 90° appears as deep in the calculation around 100 eV. At smaller angles the agreement is good for all energies with the available results [4,7] while a discrepancy is observed at larger angles. The discrepancy in the present DCS results at higher angles and the higher incident energies may be attributed to the different models used in the calculations by different authors [4,7].

For clarity, we have separated the graphical representation of the total cross sections in two figures, Figs. 4 and 5. Figure 4 shows the comparison of the present TCS generated using two models, one with the Born correction and the other without the Born correction. The calculations are carried out both for Hartree-Fock (HF) and CI models. The results of TCSs using the HF model are slightly lower than the CI model. Since CH_3OH is a polar molecule, it requires more partial waves for convergence and hence for $l > 4$ the Born correction is employed, but as is evident from the figure, the Born correction leads to a large overestimate in the TCS at low energies. The same phenomena was observed in the Born-corrected data of Bouchiha *et al.* [3] and the higher overestimation in the present case is attributed to the higher value of the dipole moment (2.28 D) used in our calculations compared to the one (1.97 D) used by Bouchiha *et al.* [3]. The overestimation could be easily understood as the Born correction is proportional to the square of the ground-state dipole moment, and the present value is 12% greater than the experimental value. Previous theoretical data were reported by Lee *et al.* [4], who employed a SCOP formalism to compute the total elastic cross sections in the range 1–500 eV. The results of Lee *et al.* [4] are higher compared with our present no Born data.

The present uncorrected (no Born) data are in fairly good agreement with the calculated total elastic cross section of Khakoo *et al.* [7] using the Schwinger multichannel method, which is in good agreement with the experimental data of Szmytkowski and Krzysztofowicz [8], Sueoka *et al.* [9], and Schmieder [10]. Khakoo *et al.* [7] obtained their low-energy data by extrapolation of the measured differential cross section (below 15°) to incorporate the backward scattering angles; this introduces very large errors in the data (of 30%–40%). The experimental data of Khakoo *et al.* [7] are higher at lower energies when compared with other experimental data presented here, which clearly reflects their difficulty in deriving TCS experiments at this energy. The discrepancy in the present data with the measured data of Khakoo *et al.* [7] decreases with increasing energy as the effect of the dipole potential decreases with an increase in the energy.

Finally, Fig. 5 shows the present data (without the Born approximation) for e-CH_3OH scattering over the entire range

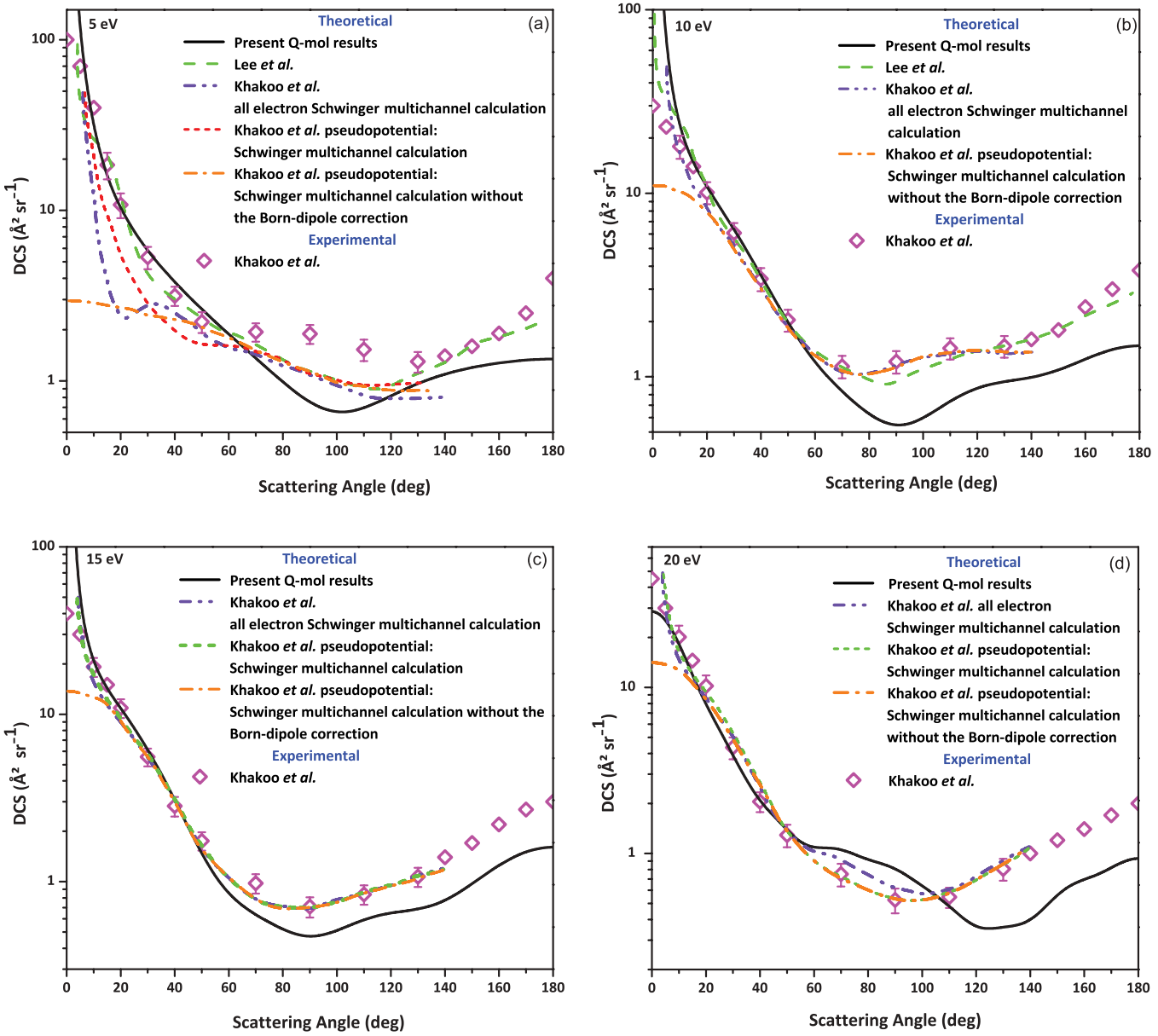

FIG. 3. (Color online) DCS of e-CH_3OH at (a) 5, (b) 10, (c) 15, and (d) 20 eV. Solid line: Present Q-mol results. Open diamond: Khakoo *et al.* [7]. Dashed-dotted-dotted line: Khakoo *et al.* [7] all-electron Schwinger multichannel calculation. Short dashed line: Khakoo *et al.* [7] pseudopotential Schwinger multichannel calculation. Dashed-dotted line: Khakoo *et al.* [7] pseudopotential Schwinger multichannel calculation without the Born-dipole correction. Dashed line: Lee *et al.* [4].

of energy studied here. The main aim here is to depict the consistency of data derived from the two formalisms (R matrix and SCOP) at the transition energy (11 eV), which enables us to provide data over an extensive energy range from meV to keV. Since a comparison of the data at low energy has already been discussed in Fig. 4, we will now compare the results at high energy. High-energy computations have been performed by three groups: Lee *et al.* [4], Khakoo *et al.* [7], and Ming and Hua [11]. The calculated values of Ming and Hua [11] are very high compared to all the other data below 20 eV. This overestimation is a result of the additivity rule used by them [11]. Beyond 20 eV, their values slowly decrease and tend to merge with the present results. In contrast, the theoretical results of Lee *et al.* [4] are in very good agreement with the present results beyond 20 eV. The computed values of Khakoo *et al.* [7] are slightly higher around threshold, but beyond the threshold their values are in better agreement. Comparing the theoretical results with the experimental data at higher energies, the results of Silva *et al.* [6], Szmytkowski and Krzysztofowicz [8], Sueoka *et al.* [9], and Schmieder [10] are in very good agreement with the present data over the complete high-energy range. This reflects the consistency of the SCOP formalism. The measured values of Khakoo *et al.* [7] show the same trend as their theoretical values for the high-energy regime. The measured values of Sugohara *et al.* [5] are lower than the other data as they obtained the total cross section by summing the integral elastic cross sections obtained by the additivity rule, and adding the total ionization cross sections

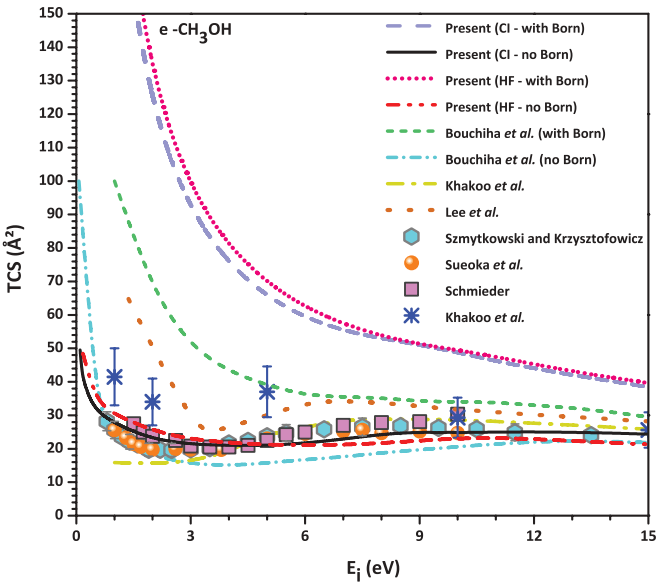

FIG. 4. (Color online) Total cross section of e-CH_3OH scattering. Solid line: Present Q-mol CI no Born results. Dashed line: Present Q-mol CI with the Born results. Short dotted line: Present Q-mol HF with Born results. Dashed-dotted-dotted line: Present Q-mol HF no Born results. Short dashed-dotted line: Bouchiha *et al.* [3] no Born. Short dashed line: Bouchiha *et al.* [3] with the Born. Dotted line: Lee *et al.* [4]. Dashed-dotted line: Khakoo *et al.* [7]. Open hexagons: Szmytkowski and Krzysztofowicz [8]. Solid spheres: Sueoka *et al.* [9]. Squares: Schmieder [10]. Asterisks: Khakoo *et al.* [7].

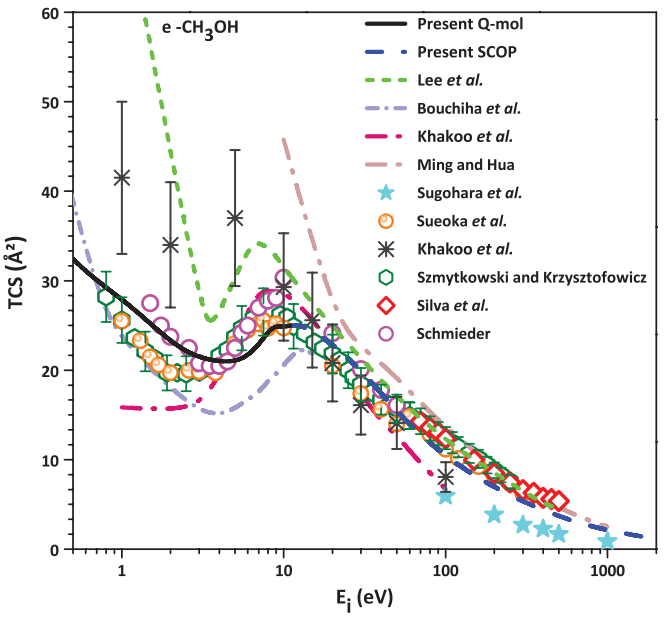

FIG. 5. (Color online) Total cross section of e-CH_3OH scattering. Solid line: Present Q-mol results. Dashed line: Present SCOP results. Short dashed-dotted line: Bouchiha *et al.* [3]. Short dashed line: Lee *et al.* [4]. Dashed-dotted line: Khakoo *et al.* [7]. Dashed-dotted-dotted line: Ming and Hua [11]. Open uptriangles: Sugohara *et al.* [5]. Open diamonds: Silva *et al.* [6]. Asterisks: Khakoo *et al.* [7]. Open hexagons: Szmytkowski and Krzysztofowicz [8]. Solid circles: Sueoka *et al.* [9]. Open squares: Schmieder [10].

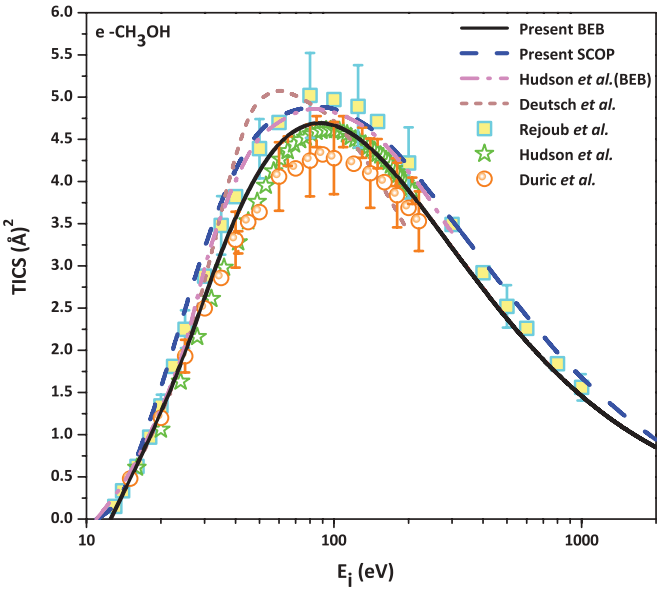

FIG. 6. (Color online) Total ionization cross section of e-CH_3OH scattering. Solid line: Present BEB results. Dashed line: Present SCOP results [33]. Dashed-dotted line: Hudson *et al.* (BEB) [55]. Short dashed line: Deutsch *et al.* [56]. Open squares: Rejoub *et al.* [52]. Open stars: Hudson *et al.* [55]. Solid spheres: Duric *et al.* [57].

of Rejoub *et al.* [52], but excluded the electronic excitation cross sections.

Finally, in order to have the complete study of e-CH_3OH scattering we also include the total ionization curve, which has already been published earlier by in Ref. [33]. The detailed discussion of the methodology is included in the previous work [33], hence we do not repeat it here. In Fig. 6 we include the calculation of the total ionization cross section using the binary Born-Bethe (BEB) method [53,54]. The present results using the BEB model are in excellent agreement with the measurements of Hudson *et al.* [55]. The measurements of Duric *et al.* [56] and Rejoub *et al.* [52] are in good accord with the present results except at the peak where the results of Duric *et al.* [56] are slightly lower, while the results of Rejoub *et al.* [52] are slightly higher than the present results. The BEB results of Hudson *et al.* [55] are slightly higher compared to the present results, and this may be attributed to the difference in the parameters used in the calculation for ionization cross sections. The results of Deutsch *et al.* [57] are shifted towards a lower energy compared to other results.

IV. CONCLUSION

An extensive theoretical study has been undertaken for e-CH_3OH scattering presenting the eigenphase, electronic excitations, and total cross sections. We demonstrate with the help of the eigenphase diagram (Fig. 1) that a CI calculation can give much more information than a simple static-exchange calculation at low energies. We can readily infer the position of resonances that may arise due to an electron interaction from these curves. We have found two Feshbach resonances in agreement with experimental data. The $2A''$ state shows a prominent structure at 8.5 eV, which is in accordance with

the earlier predicted values of 8.81 eV [3], 8.0 eV [48], and 7.9 eV [49]. Another structure is observed in the $2A'$ state cross section at 10.57 eV, which is in accord with earlier reported values of 11.73 eV [3], 10.5 eV [48], and 10.2 eV [49], which can be visualized as a peak around 11 eV in the TCS curve.

We have performed close-coupling calculations (at the static, exchange plus polarization level) employing the UK molecular R-matrix code below the ionization threshold of the target while the SCOP formalism is used beyond it. We have demonstrated through Fig. 5 that the results using these two formalisms are consistent and show a smooth transition at the overlap energy ($\sim$11 eV), confirming the validity of our theories and hence enabling us to predict the total cross sections from a low energy of 0.1 eV to a high energy of 2000 eV.

Our results are in good agreement with available data throughout the energy range. Therefore, we are confident that this methodology may be employed further to calculate the total cross sections over a wide range of energies. Such total cross-section data is important in a variety of applications from aeronomy to plasma modeling. Accordingly such a methodology may be built into the design of an online database to provide "data users" with the opportunity to request their own set of cross sections for use in their own research.

ACKNOWLEDGMENTS

M.V.K. acknowledges DST, New Delhi (SR/S2/LOP/26-2008) and C.G.L. thanks UGC, New Delhi [F. No. 40-429/2011 (SR)] for financial support under which part of this work is carried out. N.J.M. recognizes support from the EU Framework programme for the development of the VAMDC e-infrastructure.

[1] B. Block, P. Möser, and W. Hentschel, Opt. Eng. **36**, 1183 (1997).
[2] S. Y. Liao, D. M. Jiang, Q. Cheng, Z. H. Huang, and K. Zeng, Energy Fuel **20**, 84 (2006).
[3] D. Bouchiha, J. D. Gorfinkiel, L. G. Caron, and L. Sanche, J. Phys. B **40**, 1259 (2007).
[4] M.-T. Lee, G. L. C. de Souza, L. E. Machado, L. M. Brescansin, A. S. dos Santos, R. R. Lucchese, R. T. Sugohara, M. G. P. Homem, I. P. Sanches, and I. Iga, J. Chem. Phys. **136**, 114311 (2012).
[5] R. T. Sugohara, M. G. P. Homem, I. P. Sanches, A. F. de Moura, M.-T. Lee, and I. Iga, Phys. Rev. A **83**, 032708 (2011).
[6] D. G. M. Silva, T. Tejo, J. Muse, D. Romero, M. A. Khakoo, and M. C. A. Lopes, J. Phys. B **43**, 015201 (2010).
[7] M. A. Khakoo, J. Blumer, K. Keane, C. Campbell, H. Silva, M. C. A. Lopes, C. Winstead, V. McKoy, R. F. da Costa, L. G. Ferreira, M. A. P. Lima, and M. H. F. Bettega, Phys. Rev. A **77**, 042705 (2008).
[8] C. Szmytkowski and A. M. Krzysztofowicz, J. Phys. B **28**, 4291 (1995).
[9] O. Sueoka, Y. Katayama, and S. Mori, At. Collision Res. Jpn. Prog. Rep. **11**, 17 (1985).
[10] F. Schmieder, Z. Elektrochem. Angew. Phys. Chem. **36**, 700 (1930).
[11] T. Ming and W. Hua, Nucl. Instrum. Methods Phys. Res. **269**, 1094 (2011).
[12] M. Vinodkumar, C. Limbachiya, K. N. Joshipura, B. Vaishnav, and S. Gangopadhyay, J. Phys.: Conf. Ser. **115**, 012013 (2008).
[13] J. Tennyson, D. B. Brown, J. M. Munro, I. Rozum, H. N. Varambhia, and N. Vinci, J. Phys.: Conf. Ser. **86**, 012001 (2007).
[14] A. Jain, J. Chem. Phys. **86**, 1289 (1987).
[15] A. Jain and K. L. Baluja, Phys. Rev. A **45**, 202 (1992).
[16] L. E. Machado, R. T. Sugohara, A. S. dos Santos, M.-T. Lee, I. Iga, G. L. C. de Souza, M. G. P. Homem, S. E. Michelin, and L. M. Brescansin, Phys. Rev. A **84**, 032709 (2011).
[17] R. J. Buenker, G. Olbrich, H.-P. Schuchmann, B. L. Schürmann, and C. von Sonntag, J. Am. Chem. Soc. **106**, 4362 (1984).
[18] http://www.nist.gov/chemistry-portal.cfm
[19] F. W. E. Knoop, H. H. Brongersma, and L. J. Oosterhoff, Chem. Phys. Lett. **13**, 20 (1972).
[20] *Computational Methods for Electron Molecule Collisions*, edited by W. M. Huo and F. A. Gianturco (Plenum, New York, 1995).
[21] B. I. Schneider and T. N. Rescigno, Phys. Rev. A **37**, 3749 (1988).
[22] T. N. Resigno, C. W. McCurdy, A. E. Orel, and B. H. Lengsfield III, in *Computational Methods for Electron Molecule Collisions*, edited by W. M. Huo and F. Gianturco (Plenum, New York, 1995), pp. 1–44.
[23] K. Takatsuka and V. McKoy, Phys. Rev. A **24**, 2473 (1981).
[24] K. Takatsuka and V. McKoy, Phys. Rev. A **30**, 1734 (1984).
[25] A. M. Arthurs and A. Dalgarno, Proc. Phys. Soc. London, Sect. A **256**, 540 (1960).
[26] A. Faure, J. D. Gorfinkiel, L. A. Morgan, and J. Tennyson, Comput. Phys. Commun. **144**, 224 (2002).
[27] S. I. Chu and A. Dalgarno, Phys. Rev. A **10**, 788 (1974).
[28] J. Tennyson, Phys. Rep. **491**, 29 (2010).
[29] M. Vinodkumar, K. N. Joshipura, C. G. Limbachiya, and B. K. Antony, Eur. Phys. J. D **37**, 67 (2006).
[30] K. N. Joshipura, M. Vinodkumar, C. G. Limbachiya, and B. K. Antony, Phys. Rev. A **69**, 022705 (2004).
[31] C. F. Bunge, J. A. Barrientos, and A. V. Bunge, At. Data Nucl. Data Tables **53**, 113 (1993).
[32] M. Vinodkumar, C. Limbachiya, K. Korot, and K. N. Joshipura, Eur. Phys. J. D **48**, 333 (2008).
[33] M. Vinodkumar, K. Korot, and P. C. Vinodkumar, Int. J. Mass Spectrom. **305**, 26 (2011).
[34] I. Gradashteyn and I. M. Ryzhik, *Tables of Integrals, Series and Products* (Academic, New York, 1980).
[35] M. Vinodkumar, K. N. Joshipura, C. Limbachiya, and N. Mason, Phys. Rev. A **74**, 022721 (2006).
[36] S. Hara, J. Phys. Soc. Jpn. **22**, 710 (1967).
[37] X. Zhang, J. Sun, and Y. Liu, J. Phys. B **25**, 1893 (1992).
[38] G. Staszewska, D. W. Schewenke, D. Thirumalai, and D. G. Truhlar, Phys. Rev. A **28**, 2740 (1983).

[39] G. Staszewska, D. M. Schwenke, and D. G. Truhlar, J. Chem. Phys. **81**, 3078 (1984).
[40] G. Garcia and F. Blanco, Phys. Rev. A **62**, 044702 (2000).
[41] F. Blanco and G. Garcia, Phys. Rev. A **67**, 022701 (2003).
[42] C. J. Joachain, *Quantum Collision Theory* (North-Holland, Amsterdam, 1983).
[43] M. Vinodkumar, C. G. Limbachiya, K. N. Joshipura, and N. J. Mason, Eur. Phys. J. D **61**, 579 (2011).
[44] M. Vinodkumar, H. Bhutadia, B. K. Antony, and N. Mason, Phys. Rev. A **84**, 052701 (2011).
[45] M. Vinodkumar, C. G. Limbachiya, M. Y. Barot, and N. J. Mason, Eur. Phys. J. D **66**, 74 (2012).
[46] M. Vinodkumar, C. Limbachiya, and M. Barot, Molecular Physics **110**, 3015 (2012).
[47] M. Vinodkumar, A. Barot, and B. Antony, J. Chem. Phys. **136**, 184308 (2012).
[48] T. Skalick'y and M. Allan, J. Phys. B **37**, 4849 (2004).
[49] V. S. Prabhudesai, A. H. Kelkar, D. Nandi, and E. Krishnakumar, Phys. Rev. Lett. **95**, 143202 (2005).
[50] A. Kühn, H.-P. Fenzlaff, and E. Illenberger, J. Chem. Phys. **88**, 7453 (1988).
[51] M. G. Curtis and I. C. Walker, J. Chem. Soc., Faraday Trans. **88**, 2805 (1992).
[52] R. Rejoub, C. D. Morton, B. G. Lindsay, and R. F. Stebbings, J. Chem. Phys. **118**, 1756 (2003).
[53] Y.-K. Kim and M. E. Rudd, Phys. Rev. A **50**, 3954 (1994).
[54] H. Nishimura, W. M. Huo, M. A. Ali, and Y.-K. Kim, J. Chem. Phys. **110**, 3811 (1999).
[55] J. E. Hudson, M. L. Hamilton, C. Vallance, and P. W. Harland, PhysChemChemPhys **5**, 3162 (2003).
[56] N. Djuric, I. Cadez, and M. Kurepa, Fizika **21**, 339 (1989).
[57] H. Deutsch, K. Becker, R. Basner, M. Schmidt, and T. D. Märk, J. Phys. Chem. A **102**, 8819 (1998).